ISBN: 978-3-95450-236-3 ISSN: 2673-5350 doi:10.18429/JACoW-IBIC2023-TU2I02

FIRST DIRECT MEASUREMENT OF ELECTRON AND POSITRON BUNCH CHARACTERISTICS DURING POSITRON CAPTURE PROCESS AT THE POSITRON SOURCE OF THE SuperKEKB B-FACTORY

T. Suwada*, High Energy Accelerator Research Organization (KEK),
also at SOKENDAI (The Graduate University for Advanced Studies), Tsukuba, Japan

Abstract

Electron (e^-) and positron (e^+) bunch characteristics were directly measured for the first time using wideband beam monitors (WBMs) and a detection system at the e^+ source of the SuperKEKB B-factory. Both secondarily generated e^- and e^+ bunches after the e^+-production target were clearly identified during their dynamical capture process at locations of the WBMs under a two-bunch acceleration scheme. Not only the longitudinal but also transverse bunch characteristics, the time intervals between the e^- and e^+ bunches, bunch lengths, transverse bunch positions, and bunch charges were simultaneously and separately measured for each bunch as a function of the capture phase to investigate their dynamical capture process. The results show that quite symmetric dynamical behaviors for both the bunch characteristics were observed. The new WBMs open up a new window for direct measurements of both bunches during their dynamical capture process.

INTRODUCTION

High-intensity e^+ sources are indispensable and challenging in high-energy e^+e^- colliders to achieve the high luminosity required for high-energy physics experiments. In general, conventional e^+ sources [1] comprise a e^+-production target and a e^+ capture section subsequently located. Positrons are produced by impinging high-energy primary e^- beams with high intensity to a target of a high-Z material through a e^+e^- pair-production process in an electromagnetic cascade shower. The total amount of produced positrons is principally dominated by two main factors. One is the primary e^- beam power, the product of the e^- beam intensity and energy, and the other is the target characteristics of material and thickness. The resulting transverse emittances of positrons secondarily generated from the target are very large owing to the large momentum and angular spreads through an electromagnetic cascade shower process and multiple scattering in the target.

Only some parts of the positrons ejected forward are immediately captured in the e^+ capture section, in which they are focused in the transverse plane with strong axial magnetic fields, and they are captured in radio-frequency (RF) buckets of multiple accelerating structures (ACCs) in the longitudinal direction. Note that in the e^+ capture section, not only positrons but also secondarily generated electrons with approximately equivalent amounts of bunch charges simultaneously emerge from the target through this process. They are immediately and simultaneously captured in the subsequent capture section. While the e^- bunch is stopped by a beam stopper after passing the capture section, the e^+ bunch is separated from the e^- bunch and it is further accelerated by subsequent accelerating structures. After the capture section, the e^+ intensity can be measured using a beam position monitor (BPM) (or a beam intensity monitor).

An essential role of the e^+ capture section is to increase the e^+ capture efficiency as much as possible. The capture efficiency is generally simulated and optimized on the basis of beam dynamics in multidimensional transverse and longitudinal parameter spaces, which are related to electromagnetic fields of accelerating structures and magnetic fields in the capture section. Moreover, the transverse parameters of primary electrons, namely, transverse positions, injection angles, and impinging radii at the target, are also those in multidimensional parameter spaces. It is generally difficult to fully optimize the capture efficiency only by simulations. The optimization procedure should also be experimentally investigated to optimize it in multidimensional parameter spaces under realistic operation conditions.

An objective function to be optimized is only the e^+ intensity obtained after passing the e^+ capture section because no instrumentation devices are installed in it. It is generally difficult to determine not the local optimum but the global optimum in terms of the e^+ intensity with one objective function in multidimensional parameter spaces. This is because it is difficult to separately measure the e^+ and e^- bunches in the capture section by a conventional technique.

It is challenging to simultaneously and separately measure the e^+ and e^- bunch characteristics to directly verify complicated beam dynamics in the capture section and to optimize the e^+ intensity under the realistic operation condition. This is the main reason why the WBMs and detection system were developed at the e^+ source of the SuperKEKB B-factory.

HISTORICAL BACKGROUND

The purpose of introducing WBMs is to simultaneously and separately measure not only longitudinal but also transverse bunch characteristics for both e^- and e^+ bunches in the capture section. Here, I mention the background for introducing WBMs in 2018, in which preliminary investigations were started. One of the preconditions for installing any monitor in the capture section is the use of simple electromagnetic detection monitors because no advanced optical devices can be applied owing to limited installation spaces.

* tsuyoshi.suwada@kek.jp

ISBN: 978-3-95450-236-3 ISSN: 2673-5350 doi:10.18429/JACoW-IBIC2023-TU2I02

Two accelerators projects with a conventional e^+ source were developed previously. One is the SLAC linear collider (SLC) at SLAC National Accelerator Laboratory, where the commissioning of the e^+ source began in early September of 1986 [2]. The other is the advanced photon source (APS) with a e^+ storage ring at Argonne National Laboratory (ANL), where the linac commissioning began in early October of 1993 [3].

To the best of my knowledge, in 2018, there was a detection technique [2] in the time domain developed by the SLC group and another detection technique [4] in the frequency domain developed by the ANL group. A conventional button-type monitor was installed to measure both e^- and e^+ bunch intensities in the capture section of the SLC e^+ source. This monitor directly detected the signal waveforms of both bunches in the time domain immediately after the high-gradient capture section. It was difficult to separately measure them owing to both the limited frequency bandwidth and sampling frequency at that time.

On the other hand, conventional stripline-type beam position monitors were installed to measure the transverse beam positions of e^+ bunches in the capture section of the APS e^+ source. This was a e^+ source without any e^+e^- separator owing to limited installation spaces; therefore, some specific detection techniques were consequently required since it was difficult to simultaneously detect both bunches. A heterodyne technique was applied to their detection circuit using an *RF* acceleration frequency (2856 MHz). The 2856 MHz component of the detected signal with a pulse width of 30 ns was filtered, amplified, and down-converted to 70 MHz with a bandwidth of 5 MHz. The output pulses from a logarithmic amplifier were captured in track-and-hold circuits, then digitized by AD converters. Thus, since the detection circuit was based on a technique in the frequency domain, it was difficult to separately detect both bunches under mixed bunch conditions.

It is clear that if a detection technique in the time domain is chosen, several difficult issues are encountered and should be solved, that is, how to considerably reduce (or correct with high accuracy) any high-frequency signal losses in the detection circuit and transmission lines. On the other hand, if a technique in the frequency domain is chosen, we cannot separately measure any bunch characteristics. I recognized in 2019 that for this issue, a de-embedding technique [5] was critical in the detection technique in the time domain, although it was challenging.

The de-embedding technique is a mathematical procedure that removes any effects of unwanted portions of a structure, which are embedded in the measured data by subtracting their contribution. Any *RF* and microwave networks are characterized using scattering parameters (S-parameters), which are easily measured with a vector network analyzer (VNA). By applying S-parameters to any signal detection circuit and transmission lines defined as the device under test (DUT), the amplitude losses and phase distortions between the input and output of the DUT can be corrected on the basis of the de-embedding technique without adding any devices.

By way of example, I tried to measure amplitude losses and phase distortions for one of the actually applied coaxial cables, which were measured with a high-performance oscilloscope equipped with the de-embedding technique by supplying a short test pulse with a width of 30 ps at FWHM. The results showed that the output pulse was properly corrected in the time domain and it was well reproduced on the oscilloscope display in real time with nearly the same pulse height and width in comparison with the original input pulse. This was the reason why I was convinced and chose the detection technique in the time domain with the embedding technique for WBMs.

SUPERKEKB e^+ SOURCE

The SuperKEKB (SKEKB) e^+ source is one of the conventional e^+ sources and its schematic is shown in Fig. 1. Other designs have already been described in detail elsewhere [6]. Here, only an additional explanation is given. Two conventional BPMs (SP15-15 and SP16-15) and two WBMs (SP15-25 and SP16-25) were newly installed along with three horizontal and one vertical steering magnets (STX and STY, respectively) in the capture section during the summer shutdown in 2020. These steering magnets are required to correct not only the transverse orbits of the e^+ bunch due to the off-axis bombardment to the target but also any misalignments of the magnet system generating axial magnetic fields in the capture section.

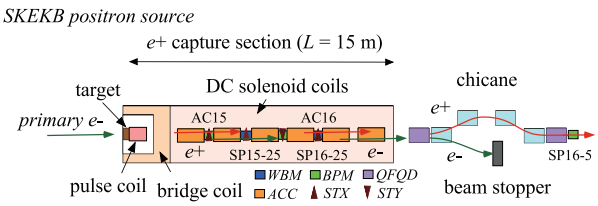

Figure 1: Schematic of the SKEKB e^+ source; QFQD: quadrupole focusing (QF) and quadrupole defocusing (QD) magnetic systems.

SP15-15 (SP15-25) is located 2.7 m (5.3 m) behind the target, and SP16-15 (SP16-25) is located 7.9 m (10.5 m) behind it. Conventional BPMs were installed to measure the transverse positions and intensity of the injection e^- bunch with conventional detection electronics. On the other hand, the WBMs with a bandwidth of ~10 GHz were used to simultaneously measure the transverse and longitudinal characteristics of both the e^- and e^+ bunches.

SIGNAL DETECTION SYSTEM

A photograph of the new beam monitor and its detection system for the two WBMs are shown in Figs. 2 (*a*) and (*b*), respectively. The total length of the monitor including two bellows and quick-release flange couplings (NW40, standard KF flange) at both ends is 431 mm, and the inner diameter is 38 mm. The inner surface of the front bellows is covered

ISBN: 978-3-95450-236-3 ISSN: 2673-5350 doi:10.18429/JACoW-IBIC2023-TU2I02

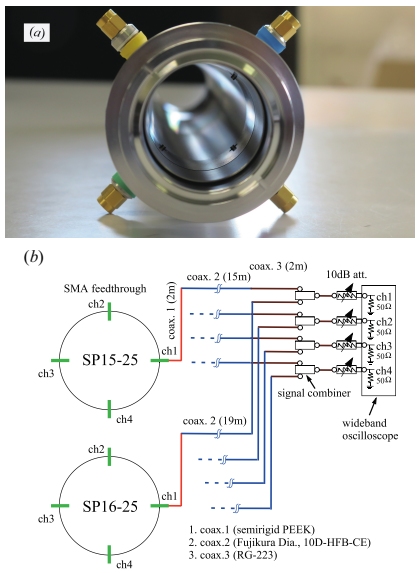

Figure 2: (a) Photograph of the WBM and (b) the detection system for the two WBMs.

with a cylindrical pipe to remove any irregularity and suppress any wakefield effects caused at the monitor front as much as possible. The pickups of the monitor are made of SMA-type vacuum feedthroughs composed of a central conductor pin made of Kovar and a dielectric substance made of ceramic. The four pickups, two horizontal and two vertical, are mounted on the upstream side of the monitor with $\pi/2$ rotational symmetry. The tips of the center pins protrude for a length of 1 mm toward the monitor center from the inner surface of the monitor.

Two sets of four signals detected with high-frequency pickups from each WBM are sent to four *RF* combiners (Marki Microwave, PD-0R618, BW0.6–18 GHz) with coaxial cables, where the eight signals are combined. A set of the combined four signals is directly sent to a wideband real-time oscilloscope (Keysight Technologies, Infiniium V DSOV134A, BW13 GHz, 40 GSa/s). The *RF* combiners are independently connected to four input channels of the oscilloscope with a fixed coaxial attenuator of 10 dB in front of each input channel, which is terminated with an internal 50-Ω terminator.

The original signal waveforms detected in the time domain are transformed to the frequency domain by applying a standard fast-Fourier transformation (FFT), and they are corrected by using the loss data on the basis of the de-embedding technique in the frequency domain. The losses for the transmission cables and *RF* combiners were measured with a VNA in advance. The corrected signal waveforms in the frequency domain were transformed to the time domain by applying an inverse FFT using a software-based Bessel filter with fourth-order roll-off at the cutoff frequency of 9.1 GHz. The corrected signal waveforms in the time domain are pulse-by-pulse displayed on the oscilloscope without any significant latency.

SIGNAL WAVEFORM ANALYSIS

The pickup signal of the WBMs is a bipolar differential signal induced by a single-bunched beam, whereas it is corrected in the frequency domain on the basis of the de-embedding technique. The typical signal waveforms detected at SP15-25 in the nominal operation are shown in Fig. 3. Figure 3(a) (Fig. 3(c)) shows the differential signal

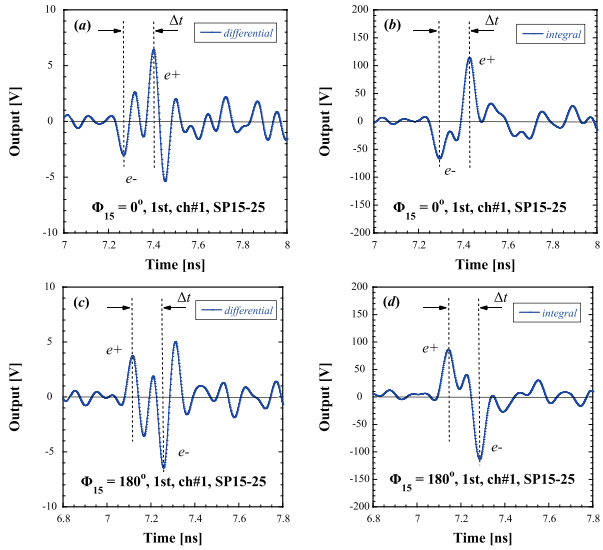

Figure 3: Typical signal waveforms (ch#1) in the nominal operation detected at SP15-25. (a) Differential waveform at $\Phi_{15} = 0^{o}$, (b) its integrated waveform, (c) differential waveform at $\Phi_{15} = 180^{o}$, and (d) its integrated waveform.

waveform of SP15-25 at $\Phi_{15} = 0^{o}$ ($\Phi_{15} = 180^{o}$) under the nominal (180° phase shifted) operation condition after the frequency correction, where Φ_{15} indicates the capture phase of AC15. Figure 3(b) (Fig. 3(d)) shows the corresponding integrated signal waveform. It is found that the signal polarity $(-, +)$ $((+, -))$ corresponds to the e^- and e^+ (e^+ and e^-) bunch signals in the time sequence, that is, the e^- (e^+) bunch precedes the e^+ (e^-) bunch in the time domain at the corresponding capture phase.

Note that the amplitude of the signal baseline before the bunch at SP15-25 is due to the intrinsic noise floor of the oscilloscope. On the other hand, the baseline level after the bunch is due to wakefields generated from upstream accelerating structures. The time interval Δt between the bunch signals can be defined by that between their peak positions from Figs. 3(b) and (d) (or Figs. 3(a) and (c)).

The bunch characteristics can be analyzed on the basis of the results of the waveform analyses. The bunch length can be defined by analyzing the pulse width in root mean square (rms) for the integrated waveform. The bunch charge can be analyzed by calculating the area properly defined in the time region of the pulsed signal. The transverse positions of the bunch can be analyzed by using the four pulsed areas obtained from four pickups on the basis of a conventional beam position analysis procedure.

ISBN: 978-3-95450-236-3 ISSN: 2673-5350 doi:10.18429/JACoW-IBIC2023-TU2I02

Thus, in terms of the e^- and e^+ bunch characteristics, the time interval, bunch lengths, transverse bunch positions, and bunch charges can be simultaneously and separately measured with WBMs. The detailed analysis and calibration procedures have already been described elsewhere [7,8] (see also references therein for an extended list).

MEASUREMENT RESULTS

Characteristic Analyses

Figure 4 shows the variations in the time interval (Δt) between the e^- and e^+ bunches at SP15-25 and SP16-25 as a function of Φ_{15} with a step phase of 10°, for which the phase Φ_{16} of AC16 was concurrently changed by the same step phase. Note that the phases $\Phi_{15} = 0°$ and $\Phi_{16} = 0°$ are defined under the nominal operation condition. It can be seen

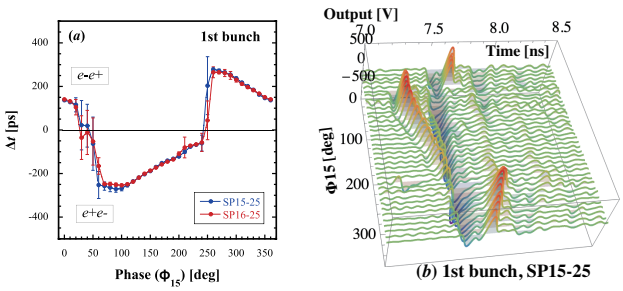

Figure 4: (*a*) Variations in Δt between the e^- and e^+ bunches as a function of Φ_{15} at SP15-25 and SP16-25. The solid curves drawn through data points are a guide to the eye. (*b*) 3D plots for the e^- and e^+ bunches at SP15-25 as a function of the phase Φ_{15} and time. The reference time is given by the arrival time of the e^- bunch.

that there are two intersections at $\Delta t = 0$ in the variations at $\Phi_{15} \simeq 50°$ and $\Phi_{15} \simeq 250°$. The results show that the line-order switch for the e^- and e^+ bunches due to their dynamical phase-slip process in the axial direction was observed as functions of the capture phase. The e^+ (e^-) bunch precedes the e^- (e^+) bunch in the phase region of $\Phi_{15} \simeq 50°$-$250°$ ($\Phi_{15} \simeq 0°$-$50°$ and $\Phi_{15} \simeq 250°$-$360°$), which corresponds to $\Delta t < 0$ ($\Delta t > 0$). This means that the e^+ and e^- bunches are in the accelerating and decelerating (decelerating and accelerating) phase regions for AC15, respectively. It can be understood that the e^+ (e^-) bunch is in the decelerating (accelerating) region under the nominal operation condition.

Figure 5 shows the variations in the transverse position displacements for the e^- and e^+ bunches at SP15-25 and SP16-25 including all the data points. Figure 5(*a*) (Fig. 5(*b*)) shows the variations for the accelerated and decelerated e^- (e^+) bunches.

It can be found that there are almost no characteristic differences in the transverse positions depending on the capture phase, even at the capture phase under the nominal operation condition and those giving the maximum charge. It is interesting that the cluster for each bunch rotates in the transverse plane owing to their cyclotron motion in the longitudinal direction between SP15-25 and SP16-25.

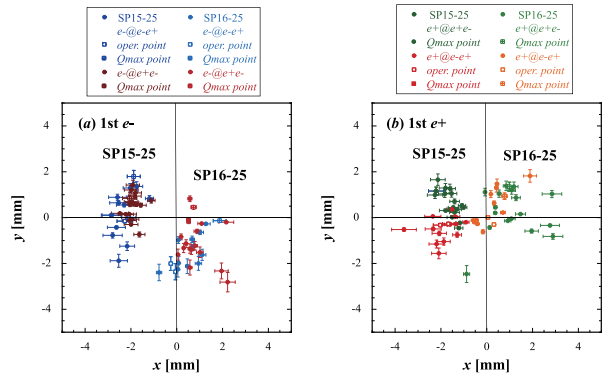

Figure 5: Variations in the transverse position displacements for the accelerated and decelerated (*a*) e^- and (*b*) e^+ bunches at SP15-25 and SP16-25 including all the data points.

Figure 6 shows the variations in the charges for the e^- and e^+ bunches at SP15-25 and SP16-25 as a function of the capture phase. Figure 6(*a*) (Fig. 6(*b*)) shows those for the e^- and e^+ bunches at SP15-25 (SP16-25). The results show

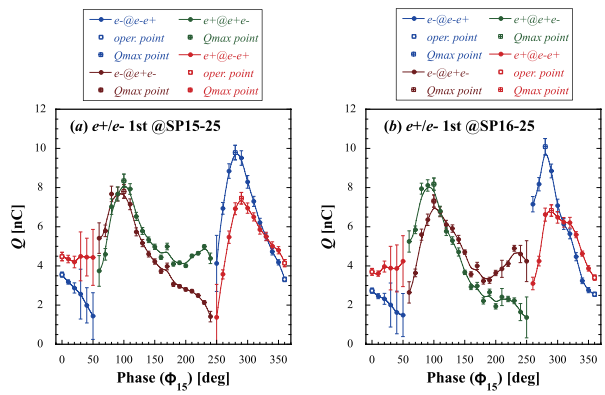

Figure 6: Variations in the bunch charges for the e^- and e^+ bunches at (*a*) SP15-25 and (*b*) SP16-25 as a function of the capture phase. The solid lines are only a guide to the eye.

that quite symmetric behaviors in terms of the variations in the charges for both the bunches are observed except for the charge excess for the e^- bunch due to the Compton effect. It can be seen that there are two capture phases in the accelerated and decelerated regions giving the maximum charge at which the capture phases for the e^- bunch agree with those for the e^+ bunch with high accuracy. It is important to point out that the charge excess at the capture phase in the accelerated region is ~20% (~10%) relative to that in the decelerated region for the e^- (e^+) bunch at SP15-25. On the other hand, the charge excess is ~27% (~17%) for the e^- (e^+) bunch at SP16-25. The results show that the accelerated bunch may be of great advantage to the decelerated bunch from the viewpoint of the bunch charge excess in the capture section.

ISBN: 978-3-95450-236-3 ISSN: 2673-5350 doi:10.18429/JACoW-IBIC2023-TU2I02

Characteristic Correlation Analyses

Δt and charges in the accelerated and decelerated e^- and e^+ bunches were simultaneously and separately measured at SP15-25 and SP16-25 including all the data points. Figure 7 shows the variations in the correlations in terms of Δt and bunch charges for the accelerated and decelerated e^- (or e^+) bunches at SP16-25 to those at SP15-25 including all the data points. Note that Δt analyzed for the e^- and e^+ bunches are the same according to their definition. Figure 7(a) shows the variations in the correlations for the accelerated and decelerated e^- bunches, and Fig. 7(b) shows those for the accelerated and decelerated e^+ bunches. It can be found

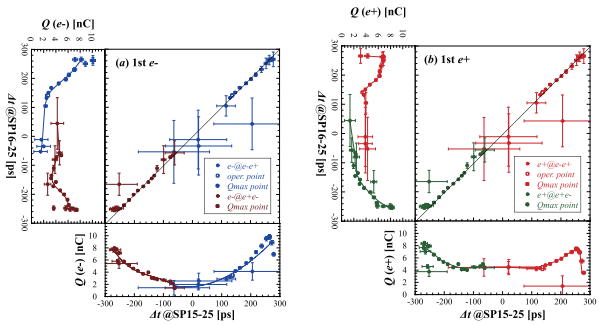

Figure 7: Variations in the correlations between Δt and charges in the accelerated and decelerated (a) e^- and (b) e^+ bunches at SP15-25 and SP16-25 including all the data points. The solid lines are only a guide to the eye.

that all the data points form a straight line tilted by 45° to the horizontal axis in the accelerated and decelerated e^- and e^+ bunches. The results again show that the phase-slip process occurs during the passage of both the bunches in AC15 and it is fixed at AC16. They also show that Δt giving the maximum charge is obtained at the nearly largest time intervals, in other words, at which the phase slip is induced to a maximum degree in AC15. The Δt values at the maximum charge are -268 ± 11 ps and 264 ± 9 ps on average for the decelerated and accelerated e^- bunches, respectively. On the other hand, the Δt values are -268 ± 11 ps and 253 ± 7 ps on average for the accelerated and decelerated e^+ bunches, respectively.

Figure 8 shows the variations in the correlations in terms of the bunch lengths and charges for the e^- and e^+ bunches at SP15-25 and SP16-25 including all the data points. Figure 8(a) (Fig. 8(b)) shows the variations for the accelerated and decelerated e^- (e^+) bunches. It is found that the data points in the correlations are on a polynomial curved line rather than on a straight line tilted by 45° to the horizontal axis in both the accelerated e^- and e^+ bunches. The result shows that although any phase-slip process halts during the passage of both the bunches in AC15, the bunch lengthening (or shortening) is generated owing to particle displacement in the bunch in the longitudinal direction in accordance with the longitudinal dynamics depending on the capture phases.

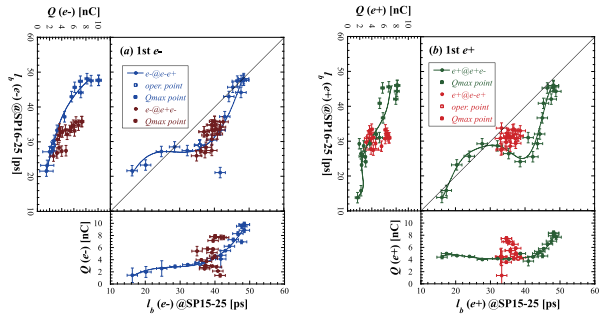

Figure 8: Variations in the correlations between the bunch lengths and charges for the accelerated and decelerated (a) e^- bunches and (b) e^+ bunches at SP15-25 and SP16-25 including all the data points. The solid lines are only a guide to the eye.

CONCLUSION

Direct simultaneous measurements of the secondarily generated e^- and e^+ bunch characteristics in the longitudinal and transverse directions were successfully performed for the first time with the WBMs and detection system under a two-bunch acceleration scheme at the e^+ capture section of the SuperKEKB B-factory. Such wideband detection techniques can be applied to conventional e^+ sources and also advanced e^+ sources in future accelerator projects. The obtained results may also improve simulations in any e^+ capture section, and thus, the e^+ intensity can be systematically and fully optimized by applying this technique along with detailed simulations in multidimensional parameter spaces towards high-intensity e^+ sources.

REFERENCES

[1] I. Chaikovska *et al.*, "Positron sources: from conventional to advanced accelerator concepts-based colliders", *J. Instrum.*, vol. 17, no. 5, pp. P05015, 2022. doi:10.1088/1748-0221/17/05/P05015

[2] J. Clendenin *et al.*, "SLC Positron Source Startup", in *Proc. LINAC'88*, Williamsburg, VA, USA, Oct. 1988, paper TH3–17, pp. 568–570.

[3] N. Galayda, "The Advanced Photon Source", in *Proc. PAC'95*, Dallas, TX, USA, May 1995, paper MAD02, pp. 4–8.

[4] R. Fuja and Y. Chung, "The APS linac beam position monitors and electronics", *AIP Conference Proceedings*, vol. 281, pp. 248–255, 1992. doi:10.1063/1.44344

[5] Keysight Technologies, Inc., Keysight Application Note 5980-2784EN.

[6] T. Kamitani *et al.*, "SuperKEKB Positron Source Construction Status", in *Proc. IPAC'14*, Dresden, Germany, Jun. 2014, pp. 579–581. doi:10.18429/JACoW-IPAC2014-MOPRI004

[7] T. Suwada *et al.*, "First simultaneous detection of electron and positron bunches at the positron capture section of the SuperKEKB factory", *Sci. Rep.*, vol. 11, pp. 12751, 2021. doi:10.1038/s41598-021-91707-0

[8] T. Suwada, "First direct measurement of electron and positron bunch characteristics at the positron source of the SuperKEKB B-factory", *AIP Advances*, vol. 13, pp. 045021, 2023. doi:10.1063/5.0145776